COMMUN. MATH. SCI.
Vol. 13, No. 2, pp. 565–575

FAST COMMUNICATION

ANALYSIS OF THE DENDRITIC INTEGRATION OF EXCITATORY AND INHIBITORY INPUTS USING CABLE MODELS*

SONGTING LI†, DOUGLAS ZHOU‡, AND DAVID CAI§

Abstract. We address the question of how a neuron integrates excitatory (E) and inhibitory (I) synaptic inputs from different dendritic sites. For an idealized neuron model with an unbranched dendritic cable, we construct its Green's function and carry out an asymptotic analysis to obtain its solutions. Using these asymptotic solutions, in the presence of E and I inputs, we can successfully reveal the underlying mechanisms of a dendritic integration rule, which was discovered in a recent experiment. Our analysis can be extended to the multi-branch case to characterize the E-I dendritic integration on any branches. The novel characterization is confirmed by the numerical simulation of a biologically realistic neuron.

Key words. Cable model, Green's function, asymptotic solution, dendritic integration.

AMS subject classifications. 35C20, 92C20.

1. Introduction

A neuron, as a fundamental unit of brain computation, exhibits great computational power in processing input signals from neighboring neurons [3, 11]. It receives thousands of spatially distributed synaptic inputs from its dendrites and then integrates them at the *soma*, leading to the neuronal information processing. This procedure is called dendritic integration. Only when the somatic membrane potential crosses a certain threshold, does the neuron initiate a spike and transmit information to downstream postsynaptic neurons via its axon. Dendritic integration rules, which determine the spike timing, are under active investigation in order to elucidate information coding in the brain.

There are two types of synaptic inputs, excitatory (E) input that induces an increase in neuronal membrane potential, known as excitatory postsynaptic potential (*EPSP*), and inhibitory (I) input that induces a decrease in neuronal membrane potential, known as inhibitory postsynaptic potential (*IPSP*). While the integration of E inputs has been extensively studied experimentally [8], E-I integration remains to be fully explored, yet are equally important for information processing in the brain [1, 9, 14]. Recently, a quantitative integration rule for a pair of E and I inputs was discovered in experiment. In the experiment [5], when an E input and an I input were elicited simultaneously at two different locations on the dendritic trunk of a rat CA1 pyramidal neuron, the summed somatic potential (*SSP*) was found to be always smaller than the linear sum of the individual *EPSP* and *IPSP* measured at the *soma*, as illustrated in figure 1.1A.

*Received: February 4, 2014; accepted (in revised form): May 17, 2014. Communicated by Shi Jin.

†Department of Mathematics, MOE-LSC and Institute of Natural Sciences, Shanghai Jiao Tong University, Shanghai, P.R. China (songting@sjtu.edu.cn).

‡Corresponding author, Department of Mathematics, MOE-LSC and Institute of Natural Sciences, Shanghai Jiao Tong University, Shanghai, P.R. China (zdz@sjtu.edu.cn).

§Corresponding author, Department of Mathematics, MOE-LSC and Institute of Natural Sciences, Shanghai Jiao Tong University, Shanghai, P.R. China and Courant Institute of Mathematical Sciences and Center for Neural Sciences, New York University, New York, NY and NYUAD Institute, New York University Abu Dhabi, PO Box 129188 Abu Dhabi, United Arab Emirates (cai@cims.nyu.edu).

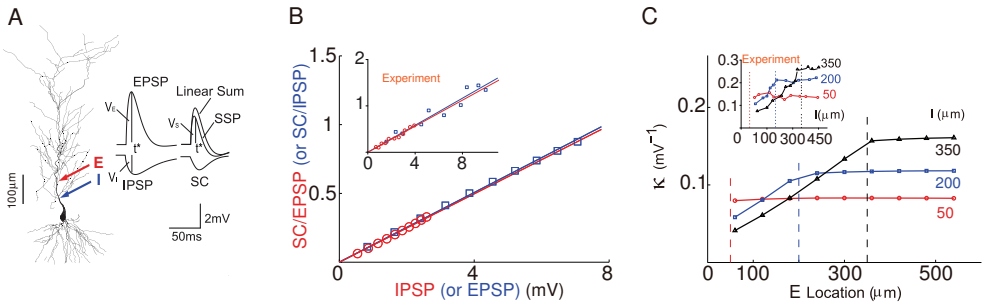

FIG. 1.1. *Dendritic integration of a pair of E-I inputs. (A) Left is a plot of a biological neuron with a pair of E-I inputs indicated by arrows. Right is an example of EPSP, IPSP, SSP, SC, and the corresponding linear sum. t^* denotes the time when EPSP reaches its peak. Note that SSP is lower than the linear sum. Figure is modified from ref. [5]. (B) Simulation results of the model (equation (2.4)) in confirmation of the rule (1.1): Ratio of SC to EPSP (SC/EPSP) plotted against IPSP (red circle) and SC/IPSP plotted against EPSP (blue square). Fixing EPSP amplitude while varying IPSP amplitude from 0.2mV to 3mV, SC/EPSP increases linearly with IPSP. Similarly, fixing IPSP amplitude while varying EPSP amplitude from 1mV to 8mV, SC/IPSP increases linearly with EPSP. Lines indicate linear fit. Stimuli are given at the locations $x_E = 300\mu m$, $x_I = 240\mu m$. Inset: experimental results (the inset is modified from ref. [5]). (C) Asymmetry of shunting coefficient κ in the model (equation (2.4)): κ as a function of distance between E location and the soma for three fixed I locations at 50 μm, 200 μm and 350 μm, respectively (marked by colored lines). Inset: experimental results for the same set of the I locations (the inset is modified from ref. [5]). The insets have the same axis labels as in the main figures. Parameters in our simulation are within the physiological regime [5, 7], $c = 1\mu F \cdot cm^{-2}$, $g_L = 0.05mS \cdot cm^{-2}$, $\varepsilon_E = 70mV$, $\varepsilon_I = -10mV$, $S = 2827.4\mu m^2$, $r_a = 100\Omega cm$, $l = 600\mu m$, $d = 1\mu m$. $\sigma_{Er} = 5ms$, $\sigma_{Ed} = 7.8ms$, $\sigma_{Ir} = 6ms$, $\sigma_{Id} = 18ms$.*

The specific arithmetic rule for the E-I integration can be summarized as follows [5]:

$$V_S = V_E + V_I + \kappa V_E V_I, \tag{1.1}$$

where V_E, V_I, and V_S are the amplitude values of the *EPSP*, *IPSP*, and *SSP* when the *EPSP* reaches its peak value. Here, $V_{SC} \equiv \kappa V_E V_I$ is the so-called shunting component (SC) with κ as the shunting coefficient. From the experiment [5], the value of κ does not depend on the amplitudes of *EPSP* and *IPSP* (as shown in the inset of figure 1.1B), but depends on the E and I input locations. In the inset of figure 1.1C, it can be seen that, for a fixed location of the I input on the dendritic trunk, κ increases as the distance between the E input and the *soma* increases when the E input is located in between the *soma* and the I input, whereas κ remains almost constant when the E input is located further away from the *soma* than the I input. This phenomenon of spatial asymmetry of κ has been incorporated into a phenomenological model [15]. However, the underlying biophysical mechanism has not been addressed.

In this work, we aim to explain the E-I dendritic integration from detailed biophysical conductance-based cable models. Although a neuron possesses complicated geometrical structures and biophysical properties, we first begin our analysis with an idealized case in which a neuron is modeled as an unbranched cylindrical dendrite connected to a spherical *soma*. This idealized system can be described by a cable equation. We obtain its Green's function and perform an asymptotic analysis. Using these asymptotic solutions, we explain theoretically the origin of the arithmetic rule (equation (1.1)) and reveal the underlying mechanism for the spatial asymmetry of κ. Next, we extend our asymptotic analysis to a more realistic model in which a neuron is endowed with multiple branched dendrites. For this general case, our analysis gives rise to a new

characterization of the shunting coefficient κ. The characterization is further confirmed by a full numerical simulation of a biologically realistic neuron.

The paper is organized as follows. In Section 2, the unbranched case is studied. We derive a one-dimensional unbranched dendritic cable model and obtain its Green's function. We then construct its asymptotic solutions and discuss the properties of the *E-I* dendritic integration. In Section 3, we extend our analysis to a multi-branch model and discuss the properties of dendritic integration for *E-I* inputs located on any branches. We present discussions and conclusions in Section 4.

2. Unbranched dendrite

A neuron is endowed with complicated dendritic morphology to process input signals from neighboring neurons. We note that the *E-I* integration investigated in the original experiment [5] was mainly focused on inputs on the main trunk of a neuron. In addition, for a large class of neurons, the tree-like dendrites can be shown to be mathematically equivalent to a single cylindrical cable [10]. We therefore first study the *E-I* dendritic integration phenomenon arising from an unbranched dendritic trunk. For the time being, we will ignore dendritic branches and will defer a discussion of a model with branches to Section 3.

2.1. The model. We consider an idealized passive neuron whose isotropic spherical *soma* is attached to an unbranched cylindrical dendrite with finite length l and diameter d. Each small segment in the neuron can be viewed as an RC circuit with a constant capacitance and leaky conductance density [4, 13]. The current conservation within a segment $[x, x+\Delta x]$ on the dendrite leads to

$$c\pi d\Delta x\frac{\partial v}{\partial t} = -g_L\pi d\Delta x v + I_{syn} + I(x) - I(x+\Delta x), \tag{2.1}$$

where v is the membrane potential with respect to the resting potential, c is the membrane capacitance density, and g_L is the leaky conductance density. Here, I_{syn} is the synaptic current

$$I_{syn} = -\sum_{q=E,I}\pi d\int_x^{x+\Delta x} G_q\cdot(v-\varepsilon_q)dx, \tag{2.2}$$

where G_E and G_I are excitatory and inhibitory synaptic conductance density and ε_E and ε_I are their reversal potentials, respectively. When an excitatory input is given at the site $x = x_E$ and an inhibitory input is given at the site $x = x_I$, we have $G_q(x,t) = f_q g_q(t)\delta(x-x_q)$, where $q = E, I$ and f_q is the input strength of synaptic conductances. The conductance is often modeled as $g_q(t) = N_q(e^{-\frac{t}{\sigma_{qd}}} - e^{-\frac{t}{\sigma_{qr}}})\Theta(t)$ with the peak value normalized to unity by the normalization factor N_q and with σ_{qr} and σ_{qd} as rise and decay time constants [7]. Here $\Theta(t)$ is a Heaviside function. The axial current $I(x)$ can be derived based on the Ohm's law,

$$I(x) = -\frac{\pi d^2}{4r_a}\frac{\partial v}{\partial x}, \tag{2.3}$$

where r_a is the axial resistivity. Taking the limit $\Delta x \to 0$, equation (2.1) becomes our unbranched dendritic cable model,

$$c\frac{\partial v}{\partial t} = -g_L v - \sum_{q=E,I} f_q g_q(t)\delta(x-x_q)(v-\varepsilon_q) + \frac{d}{4r_a}\frac{\partial^2 v}{\partial x^2}. \tag{2.4}$$

For the boundary condition of the cable model (equation (2.4)), we assume one end of the dendrite is sealed,

$$\left.\frac{\partial v}{\partial x}\right|_{x=l} = 0. \tag{2.5}$$

For the other end connecting to the *soma*, which can also be modeled as an RC circuit, by the law of current conservation, we have

$$cS\frac{\partial v^s}{\partial t} = -g_L S v^s + I_{dend}, \tag{2.6}$$

where S is the somatic membrane area, v^s is the somatic membrane potential. The dendritic current flowing to the *soma*, I_{dend}, takes the form of equation (2.3) at $x=0$. Because the voltage is continuous at the connection point, *i.e.,* $v^s(t)=v(0,t)$, we arrive at the other boundary condition at $x=0$,

$$c\frac{\partial v(0,t)}{\partial t} = -g_L v(0,t) + \frac{\pi d^2}{4Sr_a}\left.\frac{\partial v}{\partial x}\right|_{x=0}. \tag{2.7}$$

For a resting neuron, the initial condition is simply set as $v(x,0)=0$.

2.2. Green's function. In the absence of synaptic inputs, equation (2.4) is a linear system. Using a δ impulse input, its Green's function $G(x,y,t)$ can be obtained from

$$c\frac{\partial G}{\partial t} = -g_L G + \frac{d}{4r_a}\frac{\partial^2 G}{\partial x^2} + \delta(x-y)\delta(t), \tag{2.8}$$

with the following boundary conditions and initial condition,

$$c\frac{\partial G(0,y,t)}{\partial t} = -g_L G(0,y,t) + \frac{\pi d^2}{4Sr_a}\left.\frac{\partial G(x,y,t)}{\partial x}\right|_{x=0}, \quad \left.\frac{\partial G}{\partial x}\right|_{x=l} = 0, \text{ and } G(x,y,0)=0.$$

For simplicity, letting $\tau = t/c$, $\xi = x\sqrt{4r_a/d}$, $\eta = y\sqrt{4r_a/d}$, $\lambda = l\sqrt{4r_a/d}$, the solution of equation (2.8) can be obtained from the following system:

$$\frac{\partial H}{\partial \tau} = -g_L H + \frac{\partial^2 H}{\partial \xi^2} + \delta(\xi-\eta)\delta(\tau), \tag{2.9}$$

with rescaled boundary and initial conditions,

$$\frac{\partial H(0,\eta,\tau)}{\partial \tau} = -g_L H(0,\eta,\tau) + \gamma\left.\frac{\partial H(\xi,\eta,\tau)}{\partial \xi}\right|_{\xi=0}, \quad \left.\frac{\partial H}{\partial \xi}\right|_{\xi=\lambda} = 0, \text{ and } H(\xi,\eta,0)=0,$$

where $\gamma = \left(\pi d^2/2S\right)(r_a d)^{-1/2}$. Taking the Laplace transform of equation (2.9), we obtain

$$\mathcal{L}H(\xi,\eta,s) = \frac{A(\eta,s)e^{\sqrt{s+g_L}(\xi-\lambda)} + B(\eta,s)e^{\sqrt{s+g_L}(\lambda-\xi)} + e^{-\sqrt{s+g_L}|\xi-\eta|}}{2\sqrt{s+g_L}}, \tag{2.10}$$

Combining the two boundary conditions ($B(\eta,s)$ is thus eliminated), we have

$$\mathcal{L}H(\xi,\eta,s) = \begin{cases} \frac{1}{\sqrt{s+g_L}}\left[A(\eta,s)\cosh(\sqrt{s+g_L}(\lambda-\xi)) - \sinh(\sqrt{s+g_L}(\eta-\xi))\right] & \text{for } \xi \le \eta, \\ \frac{1}{\sqrt{s+g_L}}A(\eta,s)\cosh(\sqrt{s+g_L}(\lambda-\xi)) & \text{for } \xi > \eta, \end{cases} \tag{2.11}$$

where

$$A(\eta,s)=\frac{(s+g_L)\sinh(\sqrt{s+g_L}\eta)+\gamma\sqrt{s+g_L}\cosh(\sqrt{s+g_L}\eta)}{(s+g_L)\cosh(\sqrt{s+g_L}\lambda)+\gamma\sqrt{s+g_L}\sinh(\sqrt{s+g_L}\lambda)}, \tag{2.12}$$

whose denominator is denoted as $\zeta(s)$ for later discussions. For the inverse Laplace transform, we need to deal with singular points that are given by the roots of $\zeta(s)=0$. It can be easily verified that these singularities are simple poles and $\mathcal{L}H(\xi,\eta,s)$ is analytical at infinity. Then $\mathcal{L}H(\xi,\eta,s)$ can be written as

$$\mathcal{L}H(\xi,\eta,s)=\sum_n \frac{H_n(\xi,\eta)}{s+k_n}, \tag{2.13}$$

where $H_n(\xi,\eta)$ is a constant coefficient in the complex s domain, $s=-k_n$ are the singular points. Then taking the inverse Laplace transform of equation (2.13), we obtain

$$H(\xi,\eta,\tau)=\sum_n H_n(\xi,\eta)e^{-k_n\tau}. \tag{2.14}$$

Now we only need to solve k_n and $H_n(\xi,\eta)$ in equation (2.14) to obtain the Green's function of equation (2.9). We solve the singular points $s=-k_n$ first. Defining $w_n=-i\sqrt{-k_n+g_L}\lambda$, $\zeta(s)=0$ yields

$$\tan(w_n)=-\frac{w_n}{\gamma\lambda}, \tag{2.15}$$

whose roots can be determined numerically. There are solutions for w_n with $(n-1/2)\pi<w_n<(n+1/2)\pi$ for $n\geq 1$ and $w_0=0$. Next, to determine the factors $H_n(\xi,\eta)$, we use the residue theorem for integrals. For a contour C_n that winds in the counter-clockwise direction around the pole $s=-k_n$, and that does not include any other singular points, the integral of $\mathcal{L}H(\xi,\eta,s)$ on this contour is given by

$$\int_{C_n}\mathcal{L}H ds=2\pi i\left(\partial_s\frac{1}{\mathcal{L}H}\bigg|_{s=-k_n}\right)^{-1}. \tag{2.16}$$

Using equations (2.11-2.13) and (2.16), we obtain

$$H_n(\xi,\eta)=\gamma D_n\cos[w_n(1-\xi/\lambda)]\cos[w_n(1-\eta/\lambda)], \tag{2.17}$$

where $D_n=2/[\gamma\lambda+\gamma\lambda w_n^{-1}\sin(w_n)\cos(w_n)+2\cos^2(w_n)]$ for $n\geq 0$. The solution of the original Green's function for equation (2.8) can now be expressed as $G(x,y,t)=\sqrt{4r_a/(c^2d)}H(\xi,\eta,\tau)$.

2.3. Asymptotic solution. Because the synaptic currents (equation (2.2)) include the unknown dynamical variable v, the Green's function cannot be directly used to obtain the analytical solution of equation (2.4). For the physiological regime (the amplitude of an *EPSP* being less than 5mV and *IPSP* being less than 2mV), the corresponding required input strengths f_E and f_I are relatively small. Therefore, given an E input at x_E and an I input at x_I, we represent $v(x,t;x_E,x_I)$ as an asymptotic series in the powers of f_E and f_I,

$$v=\sum_{k=0}^{\infty}\sum_{m+n=k} f_E^m f_I^n v_{mn}(x,t;\mathcal{X}), \tag{2.18}$$

where $\mathcal{X} \subseteq \{x_E, x_I\}$ is the parameter space. $x_E \in \mathcal{X}$ if $m \neq 0$; $x_I \in \mathcal{X}$ if $n \neq 0$. Substituting equation (2.18) into the cable equation (2.4), order by order, we obtain a set of differential equations. For the zeroth-order, we have

$$c\frac{\partial v_{00}}{\partial t} = -g_L v_{00} + \frac{d}{4r_a}\frac{\partial^2 v_{00}}{\partial x^2}. \tag{2.19}$$

Using the boundary and initial conditions (equations (2.5) and (2.7)), the solution is simply $v_{00} = 0$. It can be interpreted as the fact that the membrane potential remains at its resting state if no stimulus is presented. For the first order of excitation $O(f_E)$,

$$c\frac{\partial v_{10}}{\partial t} = -g_L v_{10} + \frac{d}{4r_a}\frac{\partial^2 v_{10}}{\partial x^2} + g_E(t)\delta(x - x_E)\varepsilon_E, \tag{2.20}$$

with the help of Green's function, the solution can be expressed as

$$v_{10} = G(x, x_E, t) * [\varepsilon_E g_E(t)]. \tag{2.21}$$

Here '$*$' denotes convolution in time. Note that the input $\varepsilon_E g_E(t)$ at x_E can be viewed as the synaptic current when the local membrane potential is maintained at the resting state. For the second order of excitation $O(f_E^2)$,

$$c\frac{\partial v_{20}}{\partial t} = -g_L v_{20} + \frac{d}{4r_a}\frac{\partial^2 v_{20}}{\partial x^2} - g_E(t)\delta(x - x_E)v_{10}. \tag{2.22}$$

Because v_{10} is given by equation (2.21), the solution of equation (2.22) is

$$v_{20} = G(x, x_E, t) * [-g_E(t)v_{10}(x_E, t; x_E)]. \tag{2.23}$$

Note that, the second order excitatory correction in equation (2.18) has the form $f_E^2 v_{20}$. Therefore, according to equations (2.21) and (2.23), the correction is exactly the membrane potential in response to a synaptic current $-f_E g_E f_E v_{10}$, which is the product of the local conductance $f_E g_E$ with the first order local voltage $f_E v_{10}$. The above procedure and the physical interpretation of the result can be generalized to higher orders. Similarly, we can have the first and second order inhibitory solutions,

$$v_{01} = G(x, x_I, t) * [\varepsilon_I g_I(t)], \tag{2.24}$$

$$v_{02} = G(x, x_I, t) * [-g_I(t)v_{01}(x_I, t; x_I)]. \tag{2.25}$$

For the order of $O(f_E f_I)$, we have

$$c\frac{\partial v_{11}}{\partial t} = -g_L v_{11} + \frac{d}{4r_a}\frac{\partial^2 v_{11}}{\partial x^2} - g_E(t)\delta(x - x_E)v_{01} - g_I(t)\delta(x - x_I)v_{10}, \tag{2.26}$$

whose solution is obtained as follows,

$$v_{11} = G(x, x_E, t) * [-g_E(t)v_{01}(x_E, t; x_I)] + G(x, x_I, t) * [-g_I(t)v_{10}(x_I, t; x_E)]. \tag{2.27}$$

Our numerical simulation of equation (2.4) using the Crank-Nicolson method (time step $0.01ms$ and space step $1\mu m$ for all simulations) shows that the second order asymptotics is sufficiently accurate to capture the solution of membrane potentials with the realistic values of physiological parameters, as demonstrated in figure 2.1. Therefore, in the

discussion of dendritic integration below, we will invoke the approximation $v \approx V_E + V_I + V_{SC}$,

$$V_E = f_E v_{10} + f_E^2 v_{20}, \quad V_I = f_I v_{01} + f_I^2 v_{02}, \quad \text{and} \quad V_{SC} = f_E f_I v_{11} \tag{2.28}$$

where V_E and V_I are the *EPSP* and *IPSP* upon receiving an individual excitatory and inhibitory inputs, respectively. V_{SC} corresponds to the shunting component measured in experiments [5], which is the leading order of the nonlinear integration between excitation and inhibition.

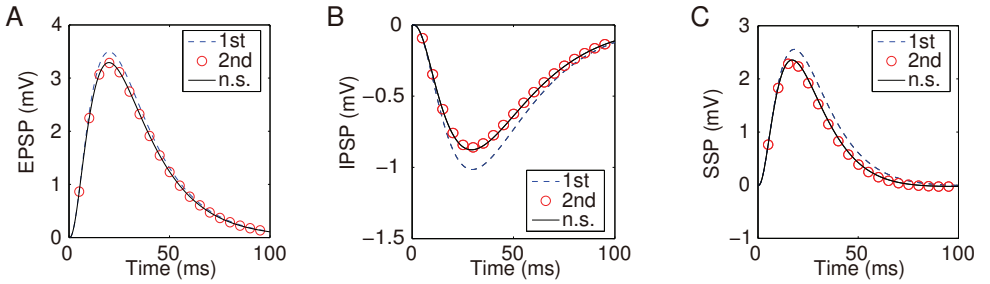

FIG. 2.1. *Asymptotic solutions of various orders for the unbranched cable model (equation (2.4)) for (A) EPSP, (B) IPSP, and (C) SSP in comparison with numerical solutions of equation (2.4). The dashed blue line is the first order approximation. The red circle is the second order approximation. The black solid line is the numerical solution of the full equation (2.4). Model parameters are the same as in figure 1.1.*

2.4. Dendritic integration. Now we use the above asymptotic solutions (equation (2.28)) to understand the *E-I* dendritic integration rule. The shunting component can be explained in our model by V_{SC} in equation (2.28). By definition, the shunting coefficient is evaluated as follows,

$$\kappa = \frac{V_{SC}}{V_E \cdot V_I} \approx \frac{v_{11}(0,t;x_E,x_I)}{v_{10}(0,t;x_E)v_{01}(0,t;x_I)}. \tag{2.29}$$

Note that the conductance strengths f_E and f_I control the membrane potential amplitudes. From equation (2.29), it can be seen that, to the leading order, κ is independent of the amplitudes of *EPSP* and *IPSP*. As has been demonstrated in our numerical simulation above, the second order asymptotic solution (equation (2.28)) is in excellent agreement with the solution of membrane potentials in the realistic physiological parameter range (figure 2.1). Therefore, the above procedure establishes the validity of the quadratic form of the arithmetic rule (1.1) and the expression of κ in terms of the solutions of the cable (equation (2.4)). Our numerical simulation of the model (equation (2.4)) further confirms the amplitude independence of κ as demonstrated in figure 1.1B.

The asymmetric spatial profile of the shunting coefficient κ (as shown in the inset of figure 1.1C) can also be understood from the asymptotic solutions. Note that, by ignoring the first term in equation (2.27) due to the fact that $\varepsilon_E = 70mV$ is almost an order of magnitude larger than $|\varepsilon_I| = 10mV$, v_{11} in equation (2.27) can be further simplified as

$$v_{11} \approx G(x,x_I,t) * [-g_I(t) v_{10}(x_I,t;x_E)], \tag{2.30}$$

which indicates that the shunting component mainly originates from the outward synaptic current, $-g_I(t)v_{10}(x_I,t;x_E)$, induced by the first order *EPSP* measured at site x_I, *i.e.,* $v_{10}(x_I,t;x_E)$. Using equation (2.30), and assuming x_I is fixed, we can rewrite κ as

$$\kappa \propto \frac{G(0,x_I,t) * [-g_I(t)v_{10}(x_I,t;x_E)]}{v_{10}(0,t;x_E)}. \tag{2.31}$$

In the small limit of the dendritic length l, from equation (2.15), we have $w_0 = 0$, $w_n \approx (n-\frac{1}{2})\pi$ for $n \geqslant 1$, which corresponds to $k_0 = g_L$, $k_n \approx \alpha w_n^2/l^2$ for $n \geqslant 1$ with $\alpha = d/4r_a$. Then, using the Green's function and equation (2.21) , we can obtain the following approximation for $v_{10}(x_I,t;x_E)$,

$$v_{10} \approx \frac{\beta}{1+\gamma l} e^{-g_L t/c} * g_E + \frac{2\beta c l g_E}{\alpha\gamma} \sum_{n=1}^{\infty} \frac{1}{w_n^2} \cos\left[w_n\left(1-\frac{x_I}{l}\right)\right] \cos\left[w_n\left(1-\frac{x_E}{l}\right)\right]. \tag{2.32}$$

where $\beta = \gamma\varepsilon_E \left(4r_a/c^2 d\right)^{1/2}$. We can further show that for $\partial^2_{x_E} v_{10}(x_I,t;x_E)$,

$$\frac{\partial^2 v_{10}}{\partial x_E^2} \approx \frac{\beta c g_E}{\alpha\gamma l}\left[\delta_c\left(\frac{x_I+x_E}{2l}\right) - \delta_c\left(\frac{x_I+x_E}{l}\right) - \delta_c\left(\frac{x_I-x_E}{2l}\right) + \delta_c\left(\frac{x_I-x_E}{l}\right)\right], \tag{2.33}$$

where the δ_c function is a Dirac comb with period 2. There is only one single δ function at $x_E = x_I$ with a negative sign for $x_{E,I} \in [0,l]$, which means $\partial_{x_E} v_{10}(x_I,t;x_E)$ is a step function of x_E. From equation (2.32), we have $\partial_{x_E} v_{10}(x_I,t;x_E) = 0$ at $x_E = l$. Thus, $\partial_{x_E} v_{10}(x_I,t;x_E)$ is a positive constant for $x_E \in [0,x_I]$ and vanishes for $x_E \in [x_I,l]$. Therefore, $v_{10}(x_I,t;x_E)$ is a piecewise linear function, increasing for x_E in between the *soma* and x_I, whereas it is constant when x_E exceeds x_I. Similarly, we can further show that $v_{10}(0,t;x_E)$ is a constant when $x_E \in [0,l]$. Combining these facts in equation (2.31) leads to the spatial asymmetry of κ in the small l limit. However, this phenomenon is general, as shown in figure 1.1C, which is obtained through our numerical simulation for a case that is beyond the asymptotic limit of small l.

For the general case, a physical intuition for the spatial asymmetry of κ can be described as follows. If we fix the inhibitory input at x_I, then $G(0,x_I,t)$ and $g_I(t)$ are fixed. Given an excitatory input at $x_E \in [0,x_I]$, the first-order membrane potential response measured at the *soma* is $v_{10}(0,t;x_E)$, and that measured at x_I is $v_{10}(x_I,t;x_E)$. As x_E approaches x_I, $v_{10}(0,t;x_E)$ decreases due to the increasing effective resistance between x_E and the *soma* as the distance increases between x_E and the *soma*. In contrast, $v_{10}(x_I,t;x_E)$ increases due to the decreasing effective resistance between x_E and x_I as the distance decreases between x_E and x_I. Therefore, according to equation (2.31), κ increases as x_E moves closer to x_I when $x_E \in [0,x_I]$. When $x_E > x_I$, both $v_{10}(0,t;x_E)$ and $v_{10}(x_I,t;x_E)$ will decrease when x_E moves further away from x_I. The decrease of the numerator and the denominator in equation (2.31) nearly cancel out, hence a near constant κ.

3. Branched dendrites

As mentioned previously, a large class of dendritic trees can be equivalently treated as an unbranched cable [10]. However, anatomical studies [6] have shown that dendritic trees of many different types of neurons do not satisfy the assumptions of the equivalent theorem. In addition, the majority of synaptic inputs are widely distributed on branches rather than on the dendritic trunk. Therefore, in this section, we study the *E-I* dendritic integration in a neuron with multiple dendritic branches.

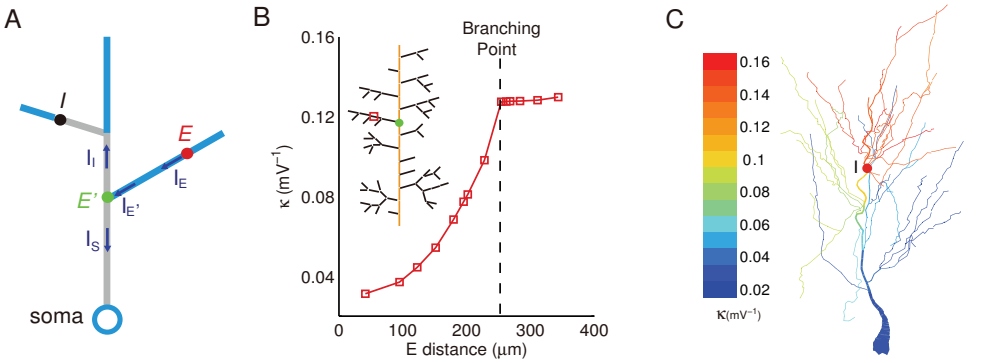

FIG. 3.1. *Spatial dependence of κ. (A) A schematic branched dendrite. (B) Spatial profiles of κ as a function of the E input location along the trunk of a realistic neuron (marked orange in the inset) for a fixed I input on a branch (red square). The dashed vertical line indicates the location of the branching point (green dot) along the trunk. (C) κ values (color-coded) for an I input (red dot) fixed at the apical trunk, with an E input scanned throughout the active dendrite (see discussions in Section 4.).*

3.1. The model. We model a realistic neuron, as shown in figure 1.1A, by a multi-branch model in which the *soma* is connected to a dendritic trunk with multiple branches attached. The dendrites consist of a set of small segments, each of which has a constant diameter and has dynamics described by the previous passive cable model (equation (2.4)). To complete the mathematical description of the branched dendrites, additional boundary conditions are prescribed at the connection site of each segment. Suppose that one end of segments $1,2,...,n$ with diameter $d_1,d_2,...,d_n$ and length $l_1,l_2,...,l_n$, respectively, are connected to the end of segment $n+1$ with diameter d_{n+1} and length l_{n+1}. Then, by the current conservation law, we have the new boundary conditions,

$$-\frac{\pi d_{n+1}^2}{4r_a}\frac{\partial v_{n+1}}{\partial x_{n+1}}\bigg|_{x_{n+1}=l_{n+1}} = -\sum_{j=1}^{n}\frac{\pi d_j^2}{4r_a}\frac{\partial v_j}{\partial x_j}\bigg|_{x_j=0}. \tag{3.1}$$

And the voltage at the connection site needs to be continuous. For the segments at the end of dendrites and the segment connecting to the *soma*, boundary conditions take the form of equations (2.5) and (2.7), respectively. In principle, Green's function can be obtained for this cable model. The analysis in Section 2 can be extended here to obtain similar asymptotic results.

3.2. Integration on branches. Previous experiments [5] have investigated the properties of κ when E and I inputs are elicited on the dendritic trunk. However, for the general situation that E and I are distributed on the branches, it remains an experimental challenge to fully elucidate κ's properties.

Our cable model predicts the properties of κ as follows. As illustrated in figure 3.1A, for a fixed I input location (marked by the black dot), the I path (marked by grey) is defined as the path between the *soma* and the I input. For any branch connecting to the I path, κ is predicted to be constant for all E sites on the branch. This can be seen as follows. First, an analysis similar to that in Section 2.4 shows that κ only depends on the input locations but not the input strengths. According to equation (2.31), κ depends on $v_{10}(0,t;x_E)$ and $v_{10}(x_I,t;x_E)$ for a fixed I site. For an arbitrary

E site (say, marked by the red dot) on a branch, during the evolution of $v_{10}(x,t;x_E)$, an axial current $\mathrm{I_E}$ is initiated by the input current $\varepsilon_E g_E(t)$ at the E site (equation (2.21)) and then flows to the remaining part of the neuron. The axial current decays to $\mathrm{I_{E'}}$ at the branching point E' (marked by the green dot). At E', $\mathrm{I_{E'}}$ splits into a flow towards *soma* denoted by $\mathrm{I_S}$ and a flow towards the I site denoted by $\mathrm{I_I}$. If we shift the stimulus location E to E' with a new input conductance at E' so as to keep $\mathrm{I_{E'}}$ unchanged, then the flows $\mathrm{I_S}$ and $\mathrm{I_I}$ remain the same. Therefore, after the stimulus site shifted, the membrane potential measured at the *soma* $v_{10}(0,t;x_E)$ and the I site $v_{10}(x_I,t;x_E)$ remains unchanged. This leads to the same value of κ at site E and E' as seen in equation (2.31).

Our numerical simulation of a cable model with realistic geometrical and biophysical property derived from the experiment [5] confirms this prediction obtained by our asymptotic analysis. NEURON software [2] is used as a numerical solver. In figure 3.1B, we fix an I input location on a branch (marked by the red square) and scan an E input location throughout the apical trunk. From figure 3.1B, it can be clearly seen that κ increases as the distance between the *soma* and E site increases, then reaches a constant as x_E moves beyond the branching point (marked by the green dot in the inset of figure 3.1B).

4. Discussion

Cable theory was developed about fifty years ago [10]. It has provided neuroscientists a powerful tool to theoretically investigate electrical properties of dendrites and membrane potential response to inputs. In general, an analytical solution can only be obtained with current injection [13] or constant conductance [12] in a direct application of Green's function method. In *vivo*, however, it is the time-varying synaptic conductance that transmits signals from dendrites to the *soma* as the case with the experimental setup [5] that we study in this work. We have developed an asymptotic method to construct its approximate solutions for the cable system under synaptic conductance inputs and have used these asymptotic solutions to reveal the physical mechanisms of the *E*-*I* dendritic integration as discovered in experiment [5]. Our asymptotic method can be naturally generalized to investigate *E*-*E* and *I*-*I* integration. We note that our analysis has only considered the passive property of a neuron. Because a neuron contains extensive active ionic channels and they play an important role in information processing during dendritic integration [3, 11], it is important to incorporate these active channels into theoretical work. One such example from our numerical study which incorporates active channels as implemented in ref. [5] is shown in figure 3.1C. It depicts a complete spatial profile of κ with the E input location scanned through all branches for a fixed I input location (marked by the red dot). We observe that on any branch connected to the I path, κ is nearly constant. Therefore, our characterization of κ remains valid even for active dendrites.

Acknowledgement. All authors are supported by the NYU Abu Dhabi Research Institute Grant No. G1301. D.Z. and D.C. by Shanghai Grant 14JC1403800, D.Z. by Shanghai Pujiang Program (Grant 10PJ1406300) & NSFC Grants 11101275 and 91230202, and D.C. by Grant NSF-DMS-1009575.

REFERENCES

[1] B. Atallah and M. Scanziani, *Instantaneous modulation of gamma oscillation frequency by balancing excitation with inhibition*, Neuron, 62, 566–577, 2009.

[2] N. Carnevale and M. Hines, *The NEURON Book*, Cambridge: Cambridge Univ. Press, 2006.

[3] H. Cuntz, M.W. Remme, and B. Torben-Nielsen, *The Computing Dendrite*, Springer, 2014.
[4] P. Dayan and L.F. Abbott, *Theoretical Neuroscience: Computational and Mathematical Modeling of Neural Systems*, Cambridge: MIT Press, 2001.
[5] J. Hao, X. Wang, Y. Dan, M. Poo, and X. Zhang, *An arithmetic rule for spatial summation of excitatory and inhibitory inputs in pyramidal neurons*, Proc. Natl. Acad. Sci. USA, 106, 21906–21911, 2009.
[6] D. Hillman, *Neuronal shape parameters and substructures as a basis of neuronal form*, The Neurosciences: Fourth Study Program,, 477–498, 1979.
[7] C. Koch, *Biophysics of Computation: Information Processing in Single Neurons*, Oxford University Press, 2004.
[8] J.C. Magee, *Dendritic integration of excitatory synaptic input*, Nature Reviews Neurosci., 1, 181–190, 2000.
[9] N. Priebe and D. Ferster, *Direction selectivity of excitation and inhibition in simple cells of the cat primary visual cortex*, Neuron, 45, 133–145, 2005.
[10] W. Rall, *Theory of physiological properties of dendrites*, Annals of the New York Academy of Sciences, 96, 1071–1092, 1962.
[11] G. Stuart, N. Spruston, and M. Häusser, *Dendrites*, Oxford: Oxford University Press, 2007.
[12] Y. Timofeeva, S.J. Cox, S. Coombes, and K. Josić, *Democratization in a passive dendritic tree: an analytical investigation*, J. Comput. Neurosci., 25, 228–244, 2008.
[13] H.C. Tuckwell, *Introduction to Theoretical Neurobiology: Volume 1, Linear Cable Theory and Dendritic Structure*, Cambridge University Press, 1988.
[14] C. Ye, M. Poo, Y. Dan, and X. Zhang, *Synaptic mechanisms of direction selectivity in primary auditory cortex*, J. Neurosci., 30, 1861–1868, 2010.
[15] D. Zhou, S. Li, X.h. Zhang, and D. Cai, *Phenomenological incorporation of nonlinear dendritic integration using integrate-and-fire neuronal frameworks*, PLoS One, 8, e53508, 2013.